Supporting Information

Electronic transport regimes through an alkoxythiolated diphenyl-2,2'-bithiophene-based molecular junction diodes: critical assessment of the thermal dependence

Giuseppina Pace [a,], Lorenzo Caranzi [a,b], Sadir Bucella [a,b], Giorgio dell'Erba,[a] Eleonora Canesi [a], Chiara Bertarelli [a,c], Mario Caironi [a,*]*

[a] Center for Nano Science and Technology @PoliMi, Istituto Italiano di Tecnologia, Via Pascoli 70/3, 20133 Milano, Italy

[b] Dipartimento di Fisica, Politecnico di Milano, P.za L. Da Vinci, 32 20133 Milano, Italy

[c] Dipartimento di Chimica, Materiali e Ing. Chimica, Politecnico di Milano, P.za L. Da Vinci, 32 20133 Milano, Italy

*email: giuseppina.pace@iit.it; mario.caironi@iit.it

Homo-Lumo determination

The energy levels of the investigated molecule were measured through Cyclic Voltammetry (CV) experiments on a non-thiolated derivative of DPBT. The molecule investigated is reported in Figure S1.

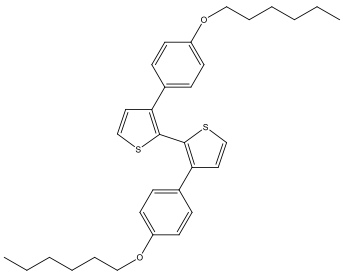

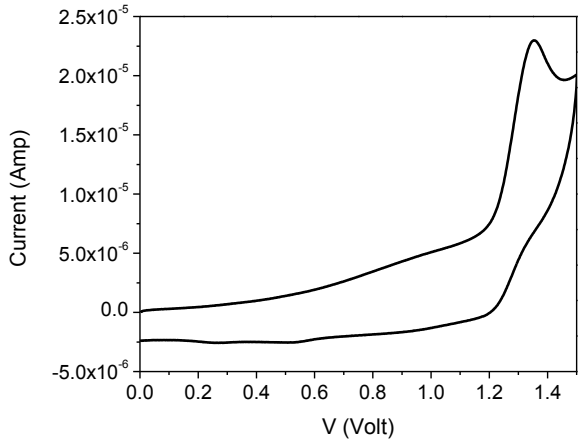

Figure S1: Molecular structure of a DPBT parent molecule and CV plot taken from solution.

The material was characterised by cyclic voltammetry, CV, at potential scan of 0.2 Vs^{-1}, in 0.5 mM solutions of the CH_2Cl_2 solvent (Sigma-Aldrich, puriss. p.a.), deaerated by N_2 purging before each experiment. 0.1 M tetrabutylammonium perchlorate, TBAP (Fluka, puriss. electrochemical grade) was used as the supporting electrolyte, in an AMEL microcell. The ohmic potential drop was compensated by the positive feedback technique. The experiments were carried out using an Autolab PGSTAT 30 potentiostat of Eco-Chemie (Utrecht, The Netherlands), run by a PC with the NOVA 1.8 software. The working electrode was a 0.071 cm^2 glassy carbon (GC) disk from Amel (Milan, Italy). The counter electrode was a platinum wire. The operating reference electrode was an aqueous saturated calomel one (SCE) with a double bridge containing a CH_2Cl_2 + 0.1 M TBAP solution, to avoid water and KCl pollution of the working solution. All the measured potentials were referred to the Fc^+/Fc couple. The intersolvental redox potential reference currently recommended by IUPAC,[1] by recording a CV scan of ferrocene in the working medium, immediately after the measurements in order to have the same experimental setup while avoiding any possible interference between the measured molecule and the redox couple. It was found that its value was fairly different from the tabulated value of −0.495 V in our CH_2Cl_2 working solution, so the measured peak potentials were referred to the values actually obtained for the Fc^+/Fc couple in the working conditions. The optimised finishing procedure for the working disk electrodes consisted in surface polishing with a diamond powder of 1 μm diameter of Aldrich on a wet DP-Nap cloth of Struers.

$E_{HOMO} = - [(E_{ox\text{-}DPBT}-E_{ox\text{-}Fc}) + 4.8]= -5.5$ eV

E_{LUMO} has been estimated from the onset of UV-vis absorption band of DPBT.

Reflection Absorption Infrared Spectroscopy (RAIRS) of DPBT SAM on Au

The presence of a Self Assembled Monolayer of the DPBT molecule on gold was proved by Reflection Absorption Infrared Spectroscopy (RAIRS) at grazing angle incidence. Comparison of the IR spectra from powder and from chemisorbed SAM on gold are reported in Figure S2. The peak assignment is presented in **Table 1**. Though the RAIRS measurements are sensitive to the orientation of the vibrational dipole moment, the use of a non flat substrate renders difficult

the assignment of the observed spectral differences between the powder and film, to a specific orientation of the molecular group with respect to the surface or to particular SAM's packing.

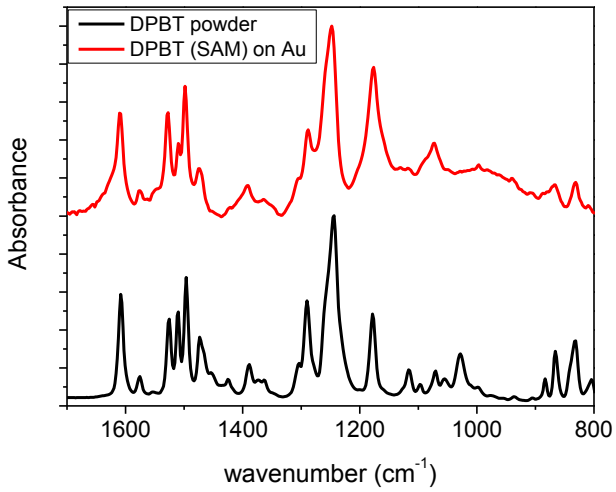

Figure S2: FT-IR spectra have been recorded: i) for powder samples, with a Nicolet FTIR Nexus spectrometer equipped with a Thermo Electron Continuμm microscope and a diamond anvil cell; ii) for SAM samples, with a Thermo Fisher Nicolet FTIR 6700 spectrometer equipped with a liquid N_2 cooled MCT detector and a Spectra-Tech FT-80 Grazing Angle accessory.

Table 1

ν (cm^{-1}) powder	ν (cm^{-1}) film	Assignement	Ref	ν (cm^{-1}) powder	ν (cm^{-1}) film	Assignement	Ref
1610	1610	Ph-ether ring str	2,2b, 3	1290-1303	1288-1303	Ph-ether str	2b, 4
1575	1575	Ph-ether ring str	2b	1243	1248	O-CH_2 twisting	4
1550	1549	C=C-H, ip, asym str, th	5	1176	1176	S-C-C, ring, ip, str	6
1510	1510	C=C-H, ip, asym str	5	1116	1118	C-O-C, op str	4
1498	1498	C=C, ip, str	7	1072	1072	C-H, ip, ben, aromatic	8
1473	1473	CH_2, CH_3 op, ben	4	1027		C=C aromatic rings, ip	7-8
1425	1423	C=C-H, ip, sym str, th ring	6	883	881	C-H, op, th ring	4
1388	1390	CH_3, ip, ben	9	865	866	C-S deformation ip, C-H ben,th	4
1363	1363	C=C, ip, str, th	6	831	831	C-H op deformation th	6

ip = in plane; op = out of plane, str = stretching; ben = bending; th = thiophene; ph = phenyl; sym = symmetric; asym = asymmetric

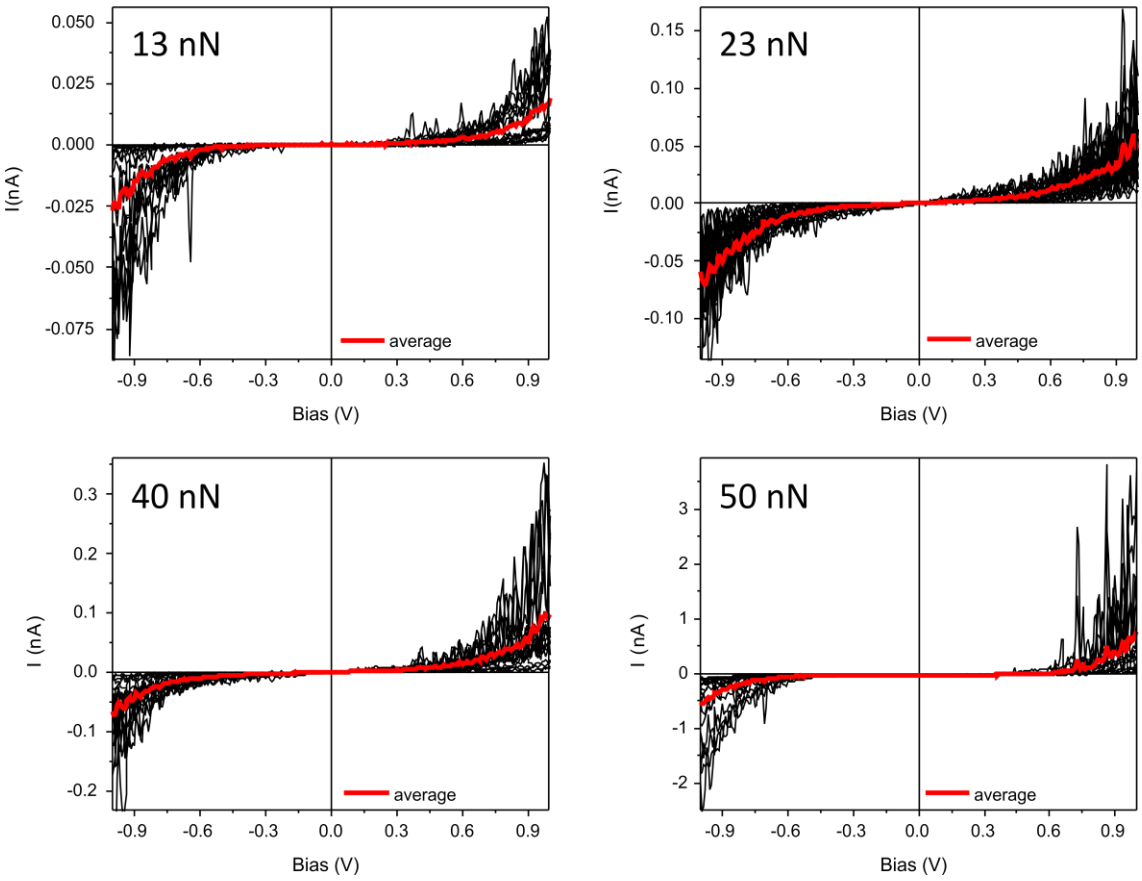

Figure S3: C-AFM I-V plots DPBT SAM on Au. Per each load the average of the multiple curves is shown by the red line.

Lock-in based conductivity measurements

We directly measured the conductivity (d*I*/d*V*) of the Au//DPBT//Au junction (Figure S3). Measurements were performed at 77 K. A transition between two transport mechanisms, given by the sharp rise in conductivity appears at around 0.3 V.

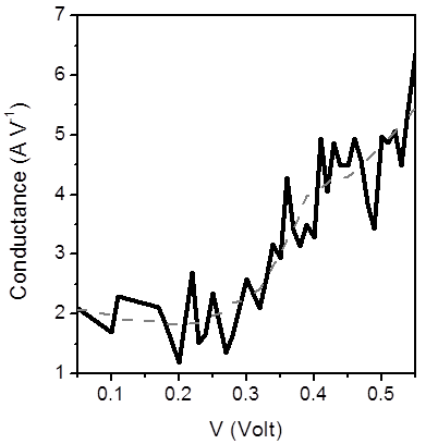

Figure S4: First harmonic (dI/dV) on PEDOT:PSS junction showing a strong electronic transition occurring at $V_T \sim 0.3$V. The dashed line represents the smoothed curve of the experimental data and helps as a guide for the eye to follow the change in conductance.

Comparing Au//C14//Au and Au//DPBT//Au junctions

In order to properly address a molecular dependent transport mechanism, and in particular the presence of a hopping mechanism, we need to be aware of possible spurious phenomena which may lead to a temperature dependent transport. In the following we compare the temperature dependent measurements of a tetradecanethiol pore junction (Au//C14//Au) with our Au//DPBT//Au one. We have to stress the point that for a roughly 2 nm thick uniform monolayer of a dielectric material a coherent tunneling mechanism would be most likely. Therefore, a completely temperature independent behavior should be observed.[10] In figure S4 we present a C14 junction where clearly a spurious mechanism is affecting the transport providing a temperature dependent current. As the alkanethiol bandgap is too large to allow a resonant transport, no molecular electronic contribution can been claimed to be responsible for such temperature dependence. Inelastic tunneling processes arising from electron-molecular phonon scattering in the SAMs would also not have such strong temperature dependence. This dependence is mostly described by a thermionic emission, while a coherent tunneling weakly comes into play only at higher biases and low temperatures. This is clearly arising from a spurious contribution, likely due to diffusion of gold atoms into the C14 monolayer. Such an

artifact can be easily found in thin (< 2 nm) Au//molecule//Au junctions. However in Figure S4 we can clearly see that for Au//DPBT//Au junction the temperature dependence does not originate from a thermionic emission at all bias and all temperature as shown for the Au//C14//Au junction. As mentioned in the main text, for Au//DPBT//Au junctions, at high bias and low temperatures a coherent tunneling is controlling the junction transport, as shown by the almost temperature independent current, while a thermionic emission is likely to characterize the transport for high bias and high temperatures. However by comparing Figure S4-c and Figure S4-f, it is clear that for low biases a thermionic emission cannot provide any good fit to the DPBT data.

We notice that at low biases in plot S4-f we find a slope inversion point. Such minima is typical for this DPBT junctions also containing PEDOT:PSS soft contact. Such slope inversion occurs at T < 280 K, exactly where the phonon assisted tunneling starts playing a role into the junction transport mechanism.

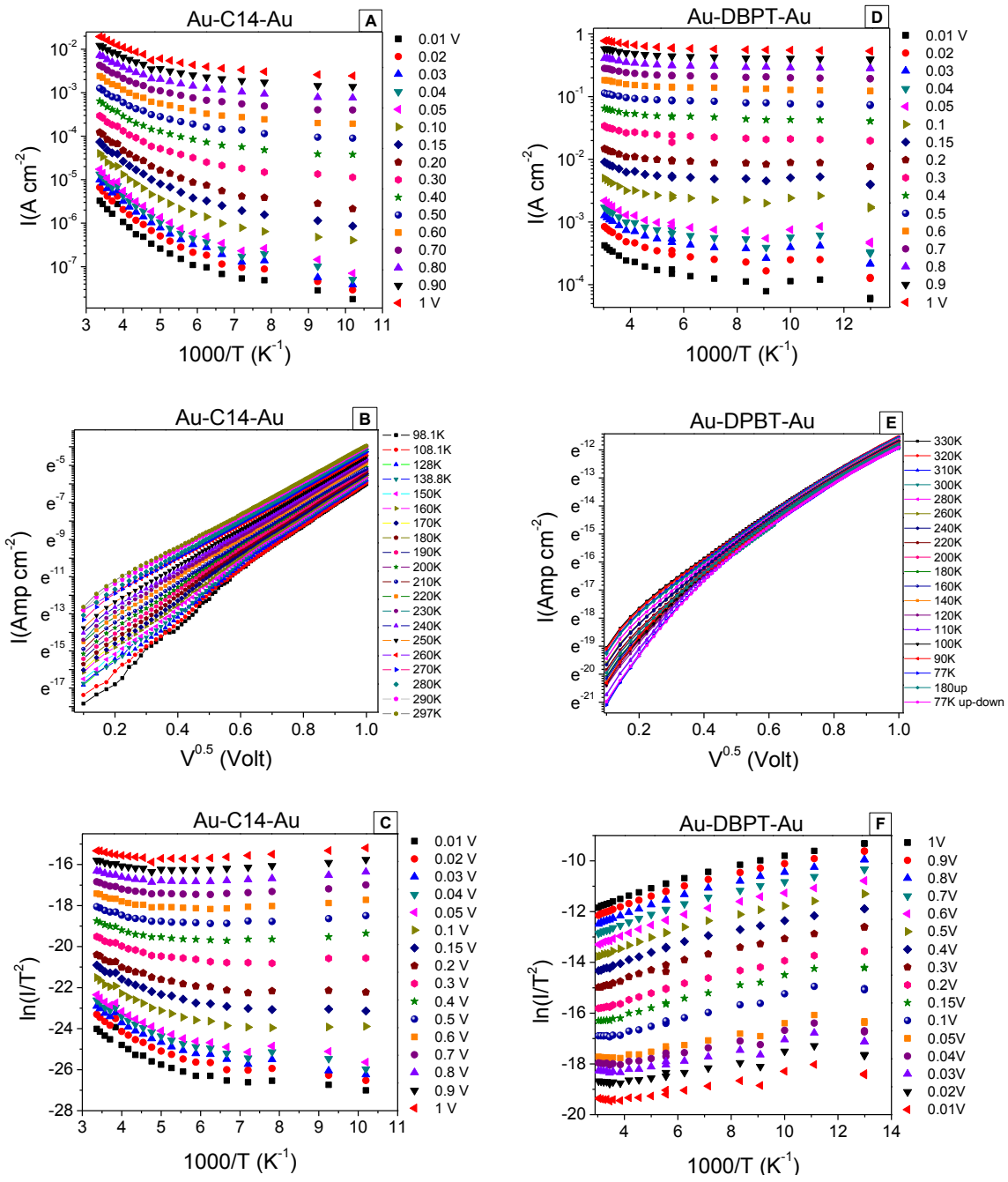

Figure S5: Comparison between Au//C14//Au and Au//DPBT//Au junctions. A and D current vs temperature dependence; B and E data plot according to thermionic emission current dependence from bias; C and F data plot according to thermionic emission from temperature. The Au//C14//Au junction has been selected among those spurious junctions where we could observe a temperature dependent conductivity, rather than a temperature independent transport as expected for a direct tunneling. A strong linearity observed over a wide temperature range demonstrates the validity of a thermionic emission.

Such linearity cannot be observed in figure E for a Au//DPBT//Au junction. In figure C we see that linearity is observed at high temperatures while for low temperatures an almost T independent process might be controlling the transport, i.e a coherent tunneling process. Both figure E and figure F show strong deviation from linearity as expected for the thermionic emission ruling the transport. The strongest deviation occurs at low biases and high temperatures. For such region we found that a hopping process is likely to occur.

Temperature dependent measurements on Au//DPBT//Au

In the following supporting material we report the temperature dependent data collected for a Au//DPBT//Au junction.

a- Metal phonons assisted tunneling

The best data fit found for the low bias and low temperature region follow power law dependence from T.

$$I \propto T^3 \exp(-\Delta E_a/KT)$$

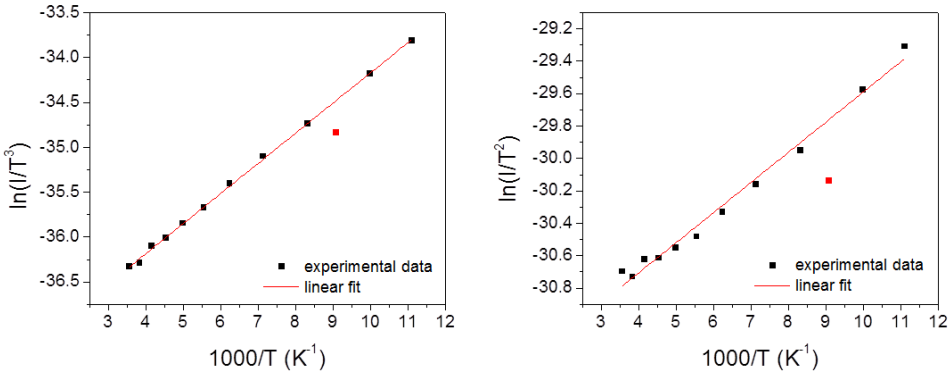

Figure S6: Best fit found for low bias and low temperature regime for Au//DPBT//Au junction at 10 mV (20 - 100 K, positive bias).

As better described in the following, the T^3 dependence can be explained by taking into account the influence of the thermally activated processes at the metal electrodes.

This thermally induced tunneling process is very similar to inorganic diodes where phonons can mediate tunneling.[11] The transition temperature between the pure hopping mechanisms to this

new phonon assisted transport regime is around 260 K. In the following we take into consideration contribution from the thermal conductivity and we derive the observed power dependence of *I* vs *T*. A proper model for the observed temperature dependence goes beyond the scope of this work; however, in the following, the important contribution of thermally induced phenomena is discussed.

b- Relating electrical conductivity (σ_{el}) to thermal conductivity (K)

For metals, the electrical conductivity dependence on temperature is different for high and low temperatures and is a function of the temperature dependence of the occupation of the phonons states. Such dependence of the resistivity ρ of a metal is given by the Bloch–Grüneisen formula:

$$\rho(T) = \rho(0) + A\left(\frac{T}{\Theta_R}\right)^n \int_0^{\frac{T}{\Theta_R}} \frac{x^n}{(e^x - 1)(1 - e^{-x})} dx$$

$\rho(0)$ = residual resistivity due to defect scattering (at low T all the phonons 'freeze'); A = constant; Θ_R = Debye temperature.

The factor n is an integer that depends upon the nature of interaction: n = 5 scattering of electrons by phonons; n = 3, s-d electron scattering; n = 2, electron–electron interaction. A linear combination of the different scattering factors can be used when more than one factor is affecting the total resistance (Matthiessen's rule).[12]

Therefore, according to the Bloch-Gruneisen formula the temperature dependence of conductivity would go as:

$$\sigma_{el} = \frac{1}{\rho} \propto \frac{1}{T^n}$$

It is already clear that the temperature dependence of the current in our junctions does not fit the prediction from the Bloch-Gruneisen theory for electron scattering.

Nevertheless, if we consider thermally induced phenomena new temperature dependence for the electron current can be found. The thermal conductivity (K) and electrical conductivity (σ_{el}) are related by the WIEDEMANN-FRANZ empirical law (valid for metals, especially noble)[12-13]:

$$K = \frac{\pi^2}{3} \cdot \frac{n\tau}{m_e} (K_B)^2 \cdot T \qquad \frac{K}{\sigma_{el}} = \frac{\pi^2}{3} \cdot \left(\frac{K_B}{e}\right)^2 \cdot T = LT$$

L = Lorenz number (2.44x10-8 WΩ K^{-2}); m_e = effective mass, K_B = Boltzmann constant; τ = average time between two collisions.

The thermal conductivity (in thermal resistance boundaries) is given by:[14]

$$K = \frac{Q}{A\nabla T} \qquad Q = \Sigma\Omega(T_2^n - T_1^n) \qquad \text{(Thermal current: } J_q = K\Delta T\text{)}$$

Q = heat/thermal flow (heat/thermal power);[11a] Ω = volume; Σ = electron-phonon coupling constant.

The coupling constant Σ and the factor n are a function of the disorder. In ordered 3D metals, (ql >1, q is the wavevector of the dominant thermal phonons, l is the mean free path for the electrons) electrons scatter mainly from phonons, in particular longitudinal acoustic phonons in which case n = 5. In the dirty limit (ql < 1) n is found to be 6, in such case scattering occurs not only from phonons, but also from impurities, defects, boundaries.[15] The factor n equals 4 when the electron-phonon scattering is a consequence of a static disorder, i.e. more likely in bulk metals. A particular case is when the mean free path for electrons (l) is of the range of sample thickness (t) so l~t, the electron-phonon scattering is also dependent on the vibrational disorder at the metal surface. In this condition, the term n in the equation for the heat flow (thermal power, Q) has been found to be $n = 5 \div n = 6$.[16]

Keeping all the above in mind, from the Wiedemann-Franz law we find for the electrical conductivity:

$$\sigma_{el} = \frac{K}{LT} = \frac{\sigma_{th}}{LT} = \frac{\alpha(T_2^n - T_1^n)}{\nabla T} \cdot \frac{1}{LT} \propto \boldsymbol{T^{n-2}}$$

At this point it is clear that the cubic dependence of the junction current on T, as observed in our experiments, is likely to be determined by thermal conductivity. Therefore, though the presence of the electric field induced by 10 mV bias, the tunneling current is mostly controlled by the temperature gradient induced between the electrodes. Heat transfer in metals is in fact promoted by electron phonon coupling and lead to the thermal diffusion of electrons. Such phonon assisted tunneling is therefore controlling the observed increase in resistance at low temperature:

$$\sigma_{exp} \propto T^3 \exp\left(\frac{\gamma}{KT}\right)$$

Therefore, we found $n = 5$ as expected for thermal conductivity in metals.

The effective electric field in the junction at 10 mV is roughly 10^5 V/cm, which is a consistent field to enable an electrical conductivity. We speculate that the low bias voltage still cannot produce a consistent current flow due to an energetic barrier (e.g. due to a strong potential drop which can occur at the Au-S interface[17]). However a thermal gradient develops between the two electrodes due to the applied bias to one end of the junction, causing an additional thermal contribution to the current which is at the base of the peculiar thermal dependence we have observed. The Wiedemann-Franz law holds when the energy of each electron is conserved in each collision therefore does not hold for inelastic processes as would be in a resonant process involving molecular levels. The diffusion of electrons trough a temperature gradient between the two electrodes is a thermodynamically driven process.[18]

Temperature dependent measurements on Au//DPBT-**PEDOT:PSS//Au**

In the following we report the transport analysis and conclusion as found for PEDOT:PSS junctions (Figure S6).

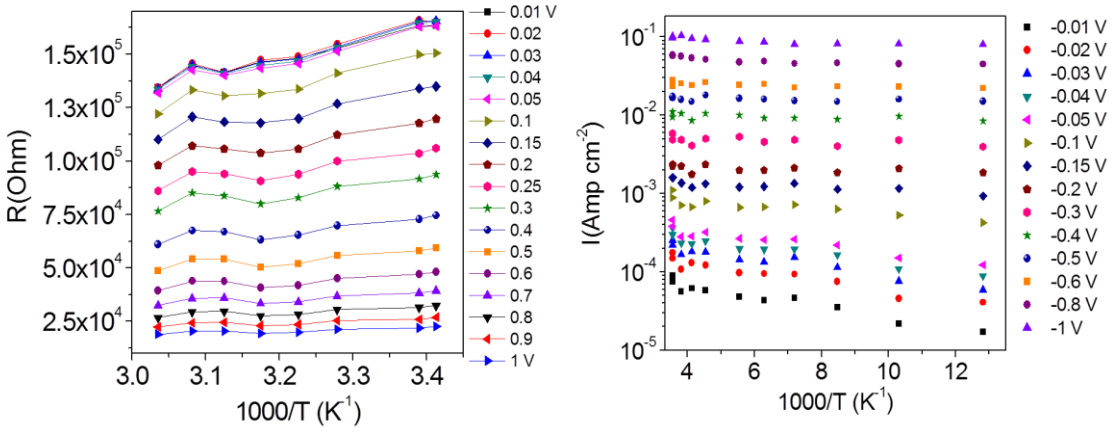

Figure S7: Temperature and bias dependent plot for Au//DPBT-PEDOT//Au junction (left 330-295 K; right 285 - 80 K).

The transition temperature between the hopping regime (activation energy 0.045 eV at 10 mV) and the phonon mediated tunneling regime occurs below 240 K. This lower activation barrier can be attributed to the new PEDOT:PSS interface which might favor the charge extraction or injection.

References

1. (a) Gritzner, G., Polarographic Half-Wave Potentials of Cations in Nonaqueous Solvents. *Pure Appl Chem* **1990,** *62* (9), 1839-1858; (b) Gritzner, G.; Kuta, J., Recommendations on Reporting Electrode-Potentials in Nonaqueous Solvents. *Denki Kagaku* **1988,** *56* (6), 398-402.
2. (a) Katash, I.; Luo, X. L.; Sukenik, C. N., Sulfonation of Alkyl Phenyl Ether Self-Assembled Monolayers. *Langmuir* **2010,** *26* (3), 1765-1775; (b) Tao, Y. T.; Wu, C. C.; Eu, J. Y.; Lin, W. L.; Wu, K. C.; Chen, C. H., Structure evolution of aromatic-derivatized thiol monolayers on evaporated gold. *Langmuir* **1997,** *13* (15), 4018-4023.
3. Cavadas, F.; Anderson, M. R., Comparison of the structure and stability of monolayers prepared with 12-phenyldodecyl mercaptan and 11-phenoxyundecyl mercaptan. *J Colloid Interf Sci* **2004,** *274* (2), 365-370.
4. Larkin, P., *Infrared and Raman Spectroscopy Principles and Spectral Interpretation* Elsevier: 2011.
5. Liedberg, B.; Yang, Z.; Engquist, I.; Wirde, M.; Gelius, U.; Gotz, G.; Bauerle, P.; Rummel, R. M.; Ziegler, C.; Gopel, W., Self-assembly of alpha-functionalized terthiophenes on gold. *J Phys Chem B* **1997,** *101* (31), 5951-5962.
6. Louarn, G.; Buisson, J. P.; Lefrant, S.; Fichou, D., Vibrational Studies of a Series of Alpha-Oligothiophenes as Model Systems of Polythiophene. *J Phys Chem-Us* **1995,** *99* (29), 11399-11404.
7. Shaporenko, A.; Brunnbauer, M.; Terfort, A.; Grunze, M.; Zharnikov, M., Structural forces in self-assembled monolayers: Terphenyl-substituted alkanethiols on noble metal substrates. *J Phys Chem B* **2004,** *108* (38), 14462-14469.
8. Stapleton, J. J.; Harder, P.; Daniel, T. A.; Reinard, M. D.; Yao, Y. X.; Price, D. W.; Tour, J. M.; Allara, D. L., Self-assembled oligo(phenylene-ethynylene) molecular electronic switch monolayers on gold: Structures and chemical stability. *Langmuir* **2003,** *19* (20), 8245-8255.
9. Rong, H. T.; Frey, S.; Yang, Y. J.; Zharnikov, M.; Buck, M.; Wuhn, M.; Woll, C.; Helmchen, G., On the importance of the headgroup substrate bond in thiol monolayers: A study of biphenyl-based thiols on gold and silver. *Langmuir* **2001,** *17* (5), 1582-1593.
10. Wang, W. Y.; Lee, T.; Reed, M. A., Mechanism of electron conduction in self-assembled alkanethiol monolayer devices. *Physical Review B* **2003,** *68* (3).
11. (a) Dubi, Y.; Di Ventra, M., Colloquium: Heat flow and thermoelectricity in atomic and molecular junctions. *Rev Mod Phys* **2011,** *83* (1), 131-155; (b) Altfeder, I.; Voevodin, A. A.; Roy, A. K., Vacuum Phonon Tunneling. *Phys Rev Lett* **2010,** *105* (16).
12. Neil W. Aschcroft, N. D. M., *Solid State Physiscs*. Hartcourt College Publishers: 1976.
13. G. V. Chester, A. T., The Law of Wiedemann and Franz *Proc. Phys. Soc.* **1961,** *77*, 1005.
14. Swartz, E. T.; Pohl, R. O., Thermal-Boundary Resistance. *Rev Mod Phys* **1989,** *61* (3), 605-668.
15. (a) Vinante, A.; Falferi, P.; Mezzena, R.; Muck, M., Hot-electron effect in palladium thin films. *Physical Review B* **2007,** *75* (10); (b) Karvonen, J. T.; Taskinen, L. J.; Maasilta, I. J., Influence of

temperature gradients on tunnel junction thermometry below 1 K: Cooling and electron-phonon coupling. *J Low Temp Phys* **2007,** *146* (1-2), 213-226.
16. Karvonen, J. T.; Taskinen, L. J.; Maasilta, I. J., Observation of disorder-induced weakening of electron-phonon interaction in thin noble-metal films. *Physical Review B* **2005,** *72* (1).
17. Holmlin, R. E.; Ismagilov, R. F.; Haag, R.; Mujica, V.; Ratner, M. A.; Rampi, M. A.; Whitesides, G. M., Correlating electron transport and molecular structure in organic thin films. *Angew Chem Int Edit* **2001,** *40* (12), 2316-+.
18. Wellstood, F. C.; Urbina, C.; Clarke, J., Hot-Electron Effects in Metals. *Physical Review B* **1994,** *49* (9), 5942-5955.